Enhanced inner core fine-scale heterogeneity towards Earth's centre

Guanning Pang, Keith D Koper, Sin-Mei Wu, Wei Wang, Marine Lasbleis, Garrett Euler

Enhanced inner core fine-scale heterogeneity towards Earth's centre

https://doi.org/10.1038/s41586-023-06213-2

Received: 9 July 2022

Accepted: 12 May 2023

Guanning Pang[1,5]✉, Keith D. Koper[1], Sin-Mei Wu[1,6], Wei Wang[2,7], Marine Lasbleis[3,8] & Garrett Euler[4]

Earth's inner core acquires texture as it solidifies within the fluid outer core. The size, shape and orientation of the mostly iron grains making up the texture record the growth of the inner core and may evolve over geologic time in response to geodynamical forces and torques[1]. Seismic waves from earthquakes can be used to image the texture, or fabric, of the inner core and gain insight into the history and evolution of Earth's core[2–6]. Here, we observe and model seismic energy backscattered from the fine-scale (less than 10 km) heterogeneities[7] that constitute inner core fabric at larger scales. We use a novel dataset created from a global array of small-aperture seismic arrays—designed to detect tiny signals from underground nuclear explosions—to create a three-dimensional model of inner core fine-scale heterogeneity. Our model shows that inner core scattering is ubiquitous, existing across all sampled longitudes and latitudes, and that it substantially increases in strength 500–800 km beneath the inner core boundary. The enhanced scattering in the deeper inner core is compatible with an era of rapid growth following delayed nucleation.

Earth's solid inner core acquires a texture, or fabric, as the mostly iron grains solidify, lithify and age. The fabric imparts seismic anisotropy through the alignment of intrinsically anisotropic crystal lattices, iron grains with preferred shapes or both[1,2]. Studies of seismic waves transmitted through the inner core (PKP_{DF}) show a surprising amount of complexity in inner core fabric[3]. The current standard model of the inner core comprises a nearly isotropic outer layer with thickness variations between quasieastern (qEH) and quasiwestern (qWH) hemispheres of approximately 50–200 km underlain by a layer reaching a depth of approximately 600–700 km beneath the inner core boundary (ICB) that has strong cylindrical anisotropy about Earth's rotation axis, surrounding an innermost inner core that has a distinct orientation of anisotropy and is slightly offset from the centre of Earth[4–6]. Continued seismic mapping of inner core fabric is important because the fabric records the history and evolution of Earth's core, which in turn, bear on the history and evolution of Earth's magnetic field, convection in the fluid outer core and heat flow into the base of the mantle.

The fine-scale structure that creates inner core fabric scatters high-frequency seismic waves, creating a long train of coda waves that follow precritical reflections from the ICB (PKiKP), known as inner core scattered (ICS) energy[7] (Fig. 1). The duration, shape and intensity of ICS depend on the properties of the inner core fabric, such as the size, shape, alignment and orientation of the solid iron grains[2,8,9]. While numerous studies have observed regional variations in the properties of waves transmitted through Earth's inner core[6], relatively few address regional variation in ICS, which provides a complementary picture of inner core fabric[10–12]. Furthermore, because of the difficulties in observing ICS energy, the geographical sampling in previous inner core scattering studies has often been spatially limited: for instance, to data from a single seismic array[13] or to localized patches of the inner core[14,15].

In this study, we use seismograms from 2,455 earthquakes recorded by a global array of 20 small-aperture seismic arrays to observe ICS energy across a nearly complete range of longitudes, at equatorial and midrange latitudes and in both polar regions (Fig. 1). Most of the seismic arrays are part of the International Monitoring System (IMS), which is operated by the Preparatory Commission for the Comprehensive Nuclear-Test-Ban Treaty Organization for the purpose of monitoring the globe for underground nuclear explosions. The arrays consist of high-quality sensors deployed in boreholes for optimal detection of short-period P waves at regional-to-teleseismic distances. We supplement the 18 IMS arrays with data from two temporary seismic deployments in Antarctica to enhance coverage in the Southern Hemisphere. The overall geometry provides unprecedented global sampling of ICS energy with corridors of crossing ray paths that promote robust observations. We use a multiple-scattering phonon approach[16] to model the observations and create a series of one-dimensional profiles of scattering strength in the inner core, which are stitched together to create a quasiglobal three-dimensional (3D) map of inner core scattering strength. The new Earth model provides fresh insight into the growth history of the inner core.

ICS energy observations

We created the ICS dataset using seismograms of moment magnitude (M_w) ≥ 5.7 earthquakes located 50°–75° away from an array. In this distance range, almost all the energy incident on the ICB is transmitted

[1]Department of Geology and Geophysics, University of Utah, Salt Lake City, UT, USA. [2]Department of Earth Sciences, University of Southern California, Los Angeles, CA, USA. [3]Laboratoire de Planétologie et Géosciences, UMR 6112, Université de Nantes, CNRS, Nantes, France. [4]Los Alamos National Laboratory, Los Alamos, NM, USA. [5]Present address: Department of Earth and Atmospheric Sciences, Cornell University, Ithaca, NY, USA. [6]Present address: Swiss Seismological Service, ETH Zurich, Zurich, Switzerland. [7]Present address: Key Laboratory of Earth and Planetary Physics, Institute of Geology and Geophysics, Chinese Academy of Sciences, Beijing, China. [8]Present address: Bureau Veritas Marine & Offshore, Paris La Défense, France. ✉e-mail: g.Pang@utah.edu

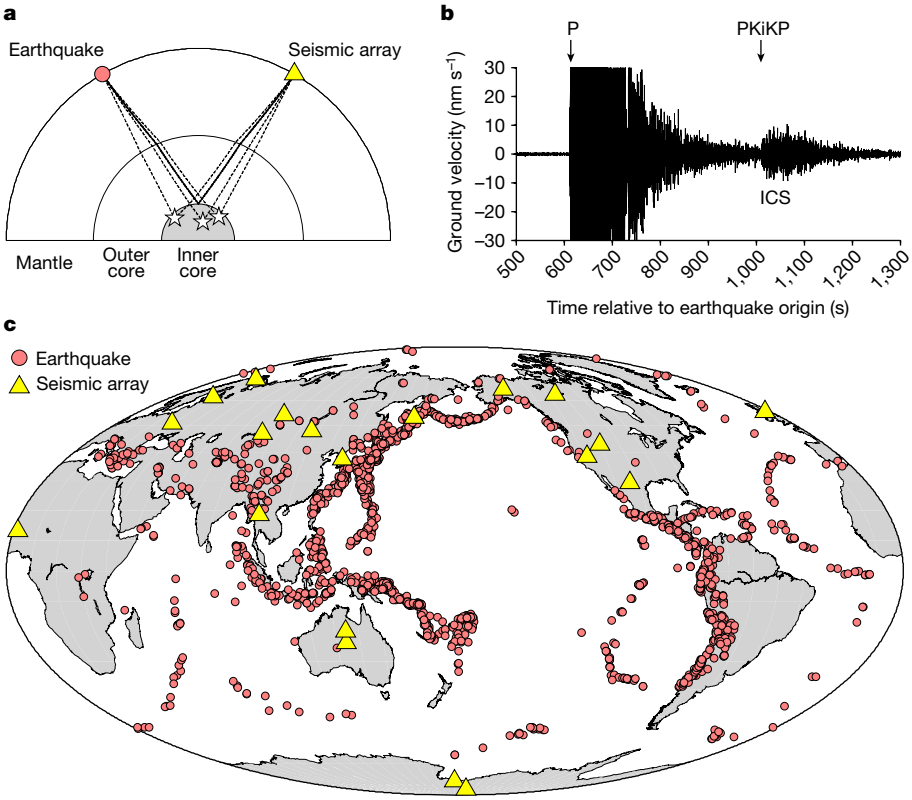

Fig. 1 | Example of ICS and map of arrays. a, Schematic cross-section illustrating the ray paths of PKiKP (solid lines) and the ICS energy (dashed lines). **b**, Example delay-and-sum beam at the ILAR seismic array in central Alaska. The beam was formed at the PKiKP slowness in a 2- to 4-Hz passband. The earthquake (M_w 6.9, 8 November 2011 02:59:08 coordinated universal time (UTC), 27.32° N, 125.62° E, 225-km depth, United States Geological Survey–National Earthquake Information Center (USGS-NEIC)) occurred northeast of Taiwan, about 64.6° away from ILAR. **c**, Map of seismic arrays and earthquakes used in this study.

across the interface[17]. The amplitude of the reflected PKiKP phase is near zero, and heterogeneity within the body of the inner core is required to generate significant PKiKP coda[15]. The arrays are appropriately sized (9–24 elements with apertures of 2–40 km) (Extended Data Fig. 1 and Extended Data Table 1) to enhance energy at the high frequencies (greater than or equal to 1 Hz) in which ICS is observed. ICS is identified at the arrays by its steep arrival direction, which is similar to the PKiKP direction of arrival. The arrays significantly enhance the signal-to-noise ratio of ICS, allowing it to be observed for hundreds of seconds (Fig. 1b).

Most of the arrays used in this study are part of the IMS, which operates in support of the Commission for the Comprehensive Nuclear-Test-Ban Treaty Organization, and meet rigorous siting and reliability requirements. IMS seismometers are commonly emplaced in boreholes in regions with low cultural noise to enhance the observability of small seismic signals produced by underground nuclear weapons tests. Many of the arrays in our study have not previously been used to study deep Earth structure. Notable examples include PS25 in Songino, Mongolia; PS26 in Torodi, Niger; PS45 in Malin, Ukraine (AKASG) and PS36 in Petropavlovsk-Kamchatskiy, Russia. The broad longitudinal coverage of the IMS arrays is important because of the quasihemispherical dichotomy in inner core structure[18]. To enhance coverage in the Southern Hemisphere, we collected data from two temporary seismometer deployments in Antarctica with small-enough aperture and high-enough station coherence to be used as teleseismic arrays (Fig. 1c).

We followed the framework presented in Wu et al.[15] for identifying and extracting ICS energy (Methods). After beamforming and slowness analysis to identify ICS, we constructed envelopes of the delay-and-sum PKiKP beams (Fig. 1b and Extended Data Fig. 2), removed the background energy corresponding to the low-slowness component of P + PcP + PP energy and stacked the denoised ICS envelopes from similar inner core geographic regions to obtain characteristic ICS envelopes (Fig. 2a). Source and receiver effects are mitigated by the beamforming, denoising, normalization and stacking procedures[15]. We find similar envelope shapes for paths that sample the same patch of the inner core with distinct source–receiver combinations (Extended Data Fig. 3), reinforcing the idea that the denoised PKiKP coda envelopes are primarily sensitive to the inner core.

We observe robust ICS envelopes for all 20 geographic regions of the inner core that were well sampled (Extended Data Fig. 4), indicating that fine-scale heterogeneity in the inner core is ubiquitous. The scattered energy initially grows for tens of seconds after the predicted PKiKP arrival before fading back into the background noise over hundreds of seconds, resulting in spindle-shaped envelopes (Fig. 2 and Extended Data Fig. 5). We characterized the envelopes with a growth time (t_{growth}), defined as the time taken from the predicted PKiKP arrival to the maximum amplitude, and a decay time (t_{decay}), defined as the time taken to decay to $1/e$ (approximately 0.37) of the maximum amplitude (Fig. 2a and Methods). Growth times ranged from 30 to 80 s, and decay times ranged from 60 to 150 s (Fig. 2). The ICS envelopes have total durations of 100–250 s if we define the duration, t_{total}, as the sum of t_{growth} and t_{decay} (Fig. 2). We emphasize that our definition of duration is designed to be independent of the background noise level and so, is necessarily conservative; it is common to observe ICS energy for 25–75 s after t_{total} (Fig. 2 and Extended Data Fig. 5).

According to elastic scattering theory, existing models of inner core heterogeneity[7,12,14] have mean free paths longer than 2,000 km;

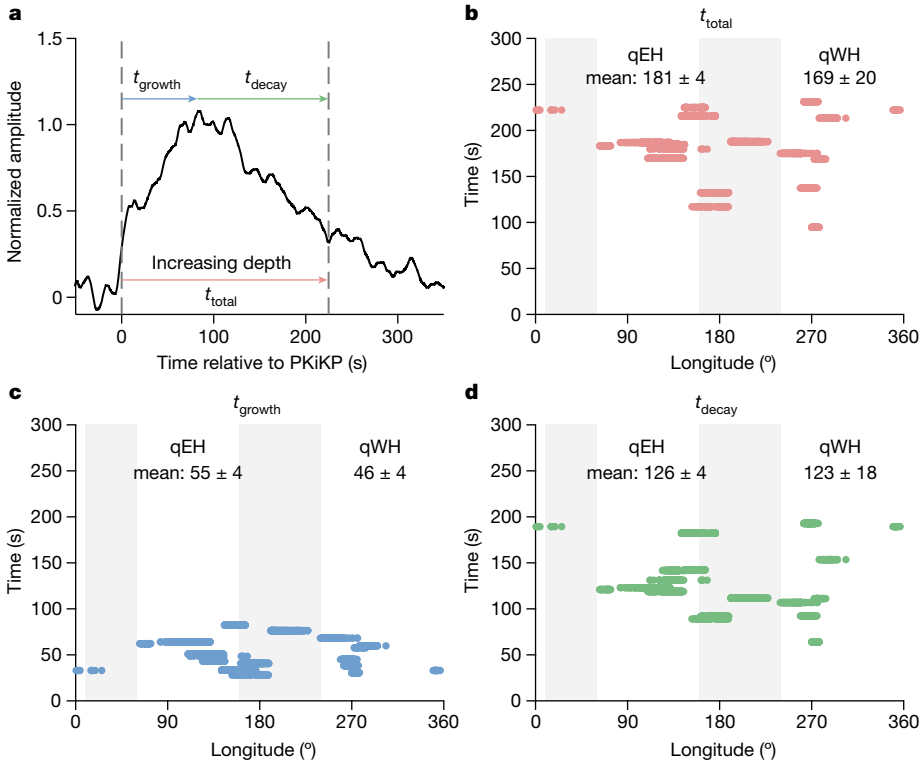

Fig. 2 | ICS energy characteristics. a, Example of a stacked PKiKP coda envelope from ILAR. The *x* axis is time relative to the predicted PKiKP arrival time. The coloured arrows indicate the duration (t_{total}), growth (t_{growth}) and decay (t_{decay}) times. **b**–**d**, These measures are also shown as a function of longitude in **b**, **c** and **d**, respectively. The grey areas illustrate the variation in published hemispherical boundaries, which range from 10° E to 60° E and 160° E to 240° E beneath Africa and the Pacific Ocean, respectively[15,19]. The mean and the standard error are reported for qEH and qWH, which are based on the measurements sampling 60° E to 160° E for the qEH and greater than or equal to 240° E for qWH.

therefore, single scattering is a good approximation, and the extraordinarily long ICS durations cannot be explained by a thin, crust-like scattering layer just beneath the ICB. The long ICS durations require that heterogeneity exists deep within the inner core. Because of the relatively high attenuation in the inner core, the scattering deep within the inner core is likely stronger than that near the ICB such that substantial ICS energy can be recorded at the surface. There is weak evidence for the qWH (greater than or equal to 240° E) having shorter-duration ICS than the qEH (60° E to 160° E) (Fig. 2); however, a Student's *t* test shows no significant difference in the means of t_{growth}, t_{decay} and t_{total} between the two hemispheres. The intrahemispherical variations in duration are comparable with the interhemispherical variations (Fig. 2 and Extended Data Fig. 5). It is also possible that geographical averaging, owing to the broad Fresnel-like sensitivity zones of hundreds of kilometres for the coda energy, would obscure a sharp boundary in our dataset if such a boundary exists in Earth[15,19].

Models of inner core heterogeneity

We modelled the ICS observations using a multiple-scattering phonon technique[16] that simulates PKiKP coda envelopes for stochastically defined distributions of inner core heterogeneity (Methods). This approach parametrizes the scattering medium using an autocorrelation function with two free parameters—the root-mean-square (RMS) variation from a reference velocity model and the spatial correlation length. These two parameters jointly determine the elastic diffusivity, *D*, which is the key parameter for quantifying the scattering strength of a heterogeneous medium[20,21] (Methods and Extended Data Fig. 6). Based on elastic scattering theory, the level of backscattered energy is typically proportional to $D^{-1.5}$, such that smaller *D* means stronger backscattering[21]. We generated a suite of 79 Earth models characterized by different diffusivities in up to three distinct inner core layers using AK135 (ref. 22) as the reference velocity model. Our simulations account for mantle scattering as well as inner core scattering, and we used the same denoising, stacking and normalization procedure on the synthetic coda envelopes as we used with the data.

We searched for the best-fitting inner core scattering model for each observed ICS envelope stack using a modified L2 norm that explicitly accounts for the growth and decay rates of the ICS envelope (Extended Data Fig. 7). We combined the elastic wave diffusivities in the uppermost 800 km of the inner core from the 20 best-fitting one-dimensional scattering models (Extended Data Fig. 5) into a 3D map of inner core heterogeneity using $D^{-1.5}$ as a proxy of scattering strength (Fig. 3). Our results indicate that fine-scale heterogeneity exists globally to depths of 500–800 km beneath the ICB (Fig. 3). Because of anelastic attenuation, we lose resolution at greater depths. The scattering strength in the uppermost 150 km of the inner core exhibits substantial lateral variations with relatively strong scattering beneath southeastern Asia, northern Latin America and south of New Zealand (Fig. 3a). There is also strong scattering beneath the northeast of Eurasia, which is consistent with recent regional mapping of inner core fine-scale heterogeneity[13]. The strong scattering beneath southeastern Asia is consistent with predictions of fast inner core growth in the past 100–300 Myr beneath the region[23]. Scattering strength 150–500 km below the ICB shows similar lateral variations with increasing scattering strength beneath the Gulf of Alaska and Atlantic Ocean (Fig. 3b,c). The regions with strong scattering spread from the centre of the qEH to the central qWH (Fig. 3), and there is only marginal evidence for a hemispherical dichotomy in scattering strength. Student's *t* tests show no significant difference in the means of $D^{-1.5}$ between hemispheres, consistent with

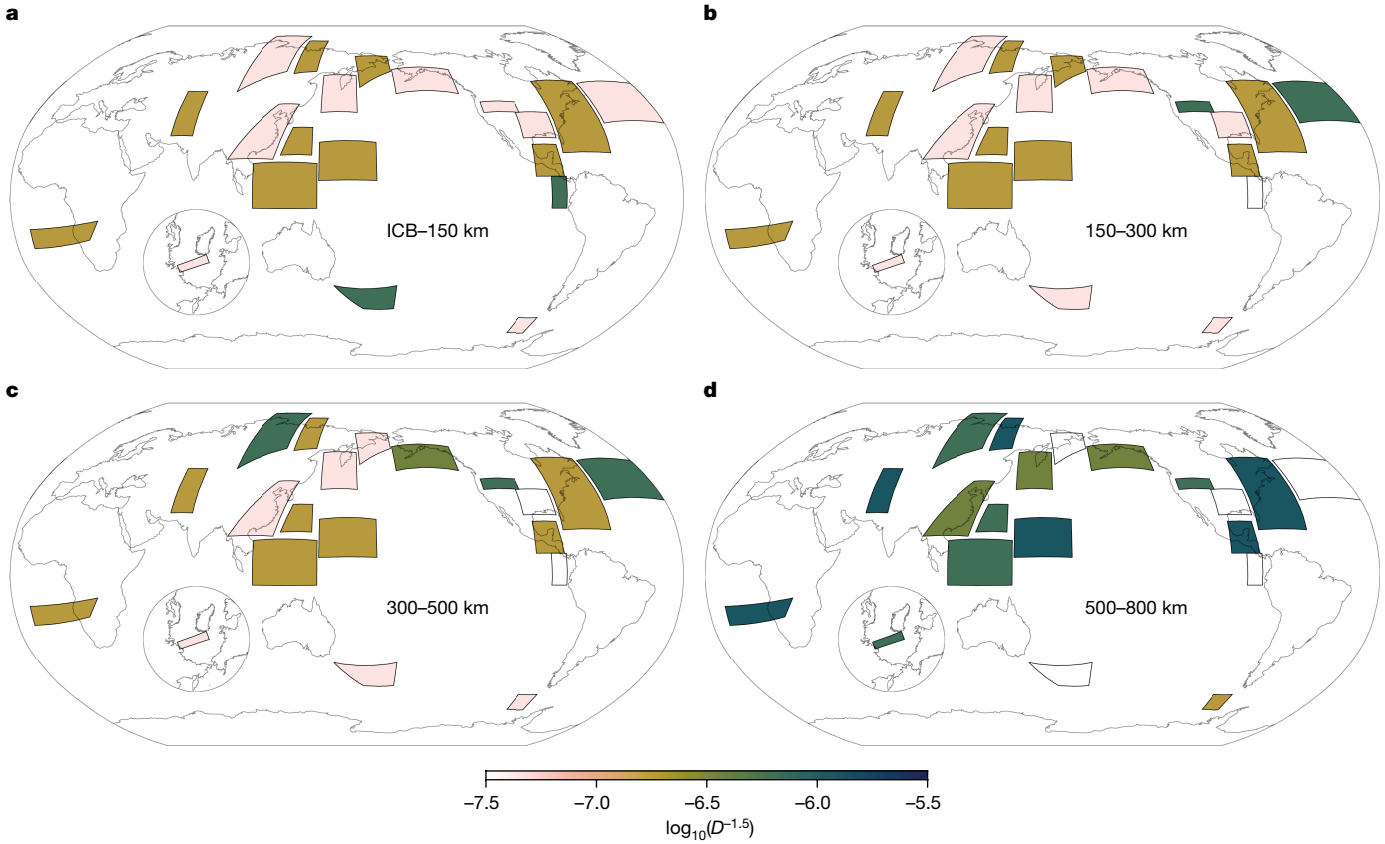

Fig. 3 | Inner core 3D scattering structure. a–d, Backscattering strength in the uppermost 150-km inner core (**a**), 150–300 km beneath the ICB (**b**), 300–500 km below the ICB (**c**) and 500–800 km below the ICB (**d**). The scattering strength is represented by $D^{-1.5}$, where D is the seismic diffusivity. Larger values of $D^{-1.5}$ mean stronger backscattered energy.

what we observed in the raw data that evidence for sharp hemispherical boundaries is insignificant (Fig. 2).

The scattering strength 500–800 km below the ICB is stronger than that in the uppermost 500 km but with weaker lateral variations (Fig. 3d). For 16 of the 20 well-sampled regions of the inner core, increasing heterogeneity strength with depth is required to match the observations. There are some small underpredictions of late coda energy for many ICS envelopes, suggesting that our models may underestimate the deeper scattering. The average elastic diffusivity (D) is approximately 1.4×10^4 m^2 s^{-1} at 700 km below the ICB, only about one third of the average value of approximately 4.9×10^4 m^2 s^{-1} at 200 km below the ICB. The average scattering strength ($D^{-1.5}$) 700 km below the ICB is about six times larger than the average scattering strength 200 km below the ICB (Fig. 4a). It is well known that coda decay rates depend on anelastic attenuation[24]; therefore, we experimented with increasing intrinsic attenuation (Q_i) from the AK135 value of 360 to 600, which is the maximum value observed in regional studies of transmitted waves. Our modelling results remained similar in the sense that stronger heterogeneity deeper in the inner core was required to match the observations. While the stronger heterogeneity deeper in the inner core is required, the sharpness of the increase is less well resolved. Smoother models involving a strong radial gradient in scattering strength cannot be excluded.

The enhanced heterogeneity can arise from changes in the size, shape, alignment or orientation of the iron grains and suggests a distinct texture within the deeper inner core[2,8,9]. Previous studies have proposed the existence of a distinct innermost inner core based on a change in the orientation of seismic anisotropy in transmitted waves[25,26]. Our observation of increased scattering 500–800 km beneath the ICB is consistent with the most recent transmitted wave study, which used a regularization-free global search methodology to estimate a depth of approximately 570 km beneath the ICB for the boundary of the innermost inner core[27]. This consistency suggests that changes in the shape, orientation or size of iron grains[9], rather than a change in lattice-preferred orientation of iron crystals, may be responsible for radial variations of anisotropy within the inner core.

Inner core nucleation and growth

Solidification texturing is the most likely micromechanism for generating fine-scale heterogeneity in the inner core. The alternative interpretation, deformational texturing, is likely too slow[28] to generate abrupt changes in seismic heterogeneity. The lateral variations of seismic heterogeneity in the uppermost 150 km of the inner core are likely imprinted by mantle-induced lateral variations in the inner core growth rate in the past 100–300 Myr (ref. 23). The deeper inner core exhibits a fossil texture[29] such that the heterogeneity structure in the deeper inner core records the history of inner core growth. The significantly enhanced fine-scale heterogeneity we observe in the deeper inner core can be interpreted as evidence for an abrupt change in the growth history of the inner core[30–32].

A plausible scenario for two-stage inner core growth involves supercooling of the primordial fluid core such that inner core formation is delayed until the nucleation barrier is overcome[30,31]. After surpassing the nucleation barrier, the inner core would initially grow very rapidly before transitioning to a steady growth regime[30] (Extended Data Fig. 8). The delayed nucleation would increase the porosity in the central part of the inner core[33], changing the volume fraction of trapped fluid and

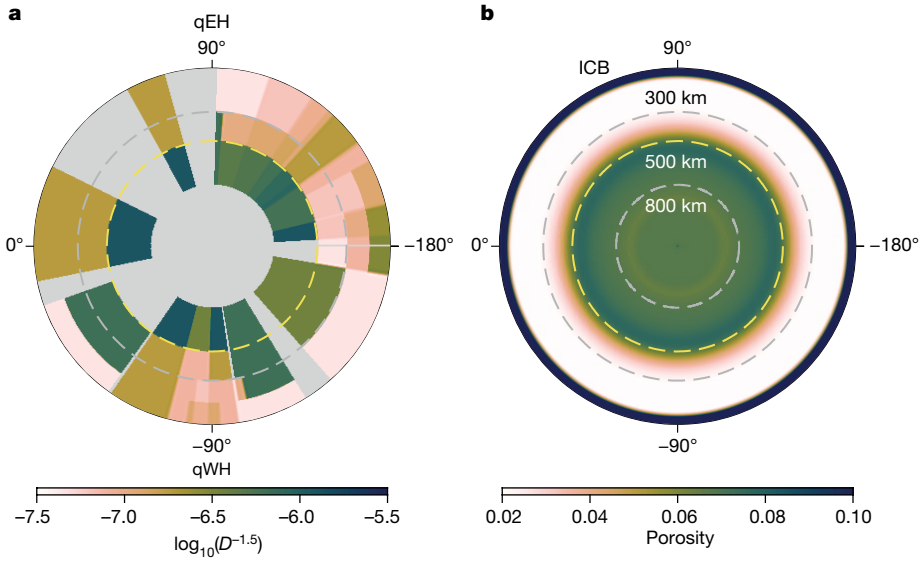

Fig. 4 | Variation of scattering strength and porosity in the equatorial plane viewed from Earth's pole. a, Global scattering variation along the inner core radius on the equatorial plane. The depths below ICB are marked as dashed circles and are labelled in **b**. The scattering strength is averaged over latitude. The grey patches indicate unconstrained portions of the inner core, either no data (patches along azimuths) or scattering is not required (patches inside inner core). **b**, Inner core porosity structure for an inner core growth model with nucleation delayed until 0.07 τ_{ic}. Yellow lines mark a depth of 500 km below ICB, where the scattering strength increases towards the deep inner core observed globally.

light elements. The trapped fluid would freeze later in time, presumably leading to a distinct texture compared with the upper part of the inner core[32], which might in principle be observed in ICS energy. We can narrow the timing of inner core nucleation by comparing our radial heterogeneity profile with the evolution of inner core porosity structure based on a simplified two-phase system driven by the density difference between liquid and solid[33]. Applying this model (Methods), the increase in heterogeneity 500–800 km below the ICB suggests that the timing of the delayed nucleation is approximately 0.07–0.12 τ_{ic}, where τ_{ic} is the presumed inner core age in the canonical growth model, which ignores the nucleation barrier[34] (Fig. 4 and Extended Data Fig. 9). The corresponding initial inner core radius at the end of the fast-growth stage is between 0.35 and 0.43 R_{ICB}, corresponding to a supercooling temperature of 20–33 K during inner core nucleation[30] (Extended Data Fig. 8).

Online content

Any methods, additional references, Nature Portfolio reporting summaries, source data, extended data, supplementary information, acknowledgements, peer review information; details of author contributions and competing interests; and statements of data and code availability are available at https://doi.org/10.1038/s41586-023-06213-2.

1. Deguen, R. Structure and dynamics of Earth's inner core. *Earth Planet. Sci. Lett.* **333**, 211–225 (2012).
2. Cormier, V. F. Texture of the uppermost inner core from forward-and back-scattered seismic waves. *Earth Planet. Sci. Lett.* **258**, 442–453 (2007).
3. Sun, X. & Song, X. Tomographic inversion for three-dimensional anisotropy of Earth's inner core. *Phys. Earth Planet. Inter.* **167**, 53–70 (2008).
4. Deuss, A. Heterogeneity and anisotropy of Earth's inner core. *Annu. Rev. Earth Planet. Sci.* **42**, 103–126 (2014).
5. Souriau, A & Calvet, M. *Treatise on Geophysics* 2nd edn, Vol. 1 (ed. Schubert, G.) Ch. 1.23 (Elsevier, 2015).
6. Tkalčić, H. Complex inner core of the Earth: the last frontier of global seismology. *Rev. Geophys.* **53**, 59–94 (2015).
7. Vidale, J. E. & Earle, P. S. Fine-scale heterogeneity in the Earth's inner core. *Nature* **404**, 273–275 (2000).
8. Monnereau, M., Calvet, M., Margerin, L. & Souriau, A. Lopsided growth of Earth's inner core. *Science* **328**, 1014–1017 (2010).
9. Calvet, M. & Margerin, L. Shape preferred orientation of iron grains compatible with Earth's uppermost inner core hemisphericity. *Earth Planet. Sci. Lett.* **481**, 395–403 (2018).
10. Koper, K. D., Franks, J. M. & Dombrovskaya, M. Evidence for small-scale heterogeneity in Earth's inner core from a global study of PKiKP coda waves. *Earth Planet. Sci. Lett.* **228**, 227–241 (2004).
11. Leyton, F. & Koper, K. D. Using *PKiKP* coda to determine inner core structure. 2. Determination of Q_c. *J. Geophys. Res. Solid Earth* **112**, B05317 (2007).
12. Peng, Z., Koper, K. D., Vidale, J. E., Leyton, F., & Shearer, P. Inner-core fine-scale structure from scattered waves recorded by LASA. *J. Geophys. Res. Solid Earth* **113**, B09312 (2008).
13. Wang, W. & Vidale, J. E. An initial map of fine-scale heterogeneity in the Earth's inner core. *Nat. Geosci.* **15**, 240–244 (2022).
14. Wu, W. & Irving, J. C. Using PKiKP coda to study heterogeneity in the top layer of the inner core's western hemisphere. *Geophys. J. Int.* **209**, 672–687 (2017).
15. Wu, S. M., Pang, G., Koper, K. D. & Euler, G. A search for large-scale variations in the fine-scale structure of Earth's inner core. *J. Geophys. Res. Solid Earth* **127**, e2022JB024420 (2022).
16. Shearer, P. M. & Earle, P. S. The global short-period wavefield modelled with a Monte Carlo seismic phonon method. *Geophys. J. Int.* **158**, 1103–1117 (2004).
17. Souriau, A. & Souriau, M. Ellipticity and density at the inner core boundary from subcritical PKiKP and PcP data. *Geophys. J. Int.* **98**, 39–54 (1989).
18. Tanaka, S. & Hamaguchi, H. Degree one heterogeneity and hemispherical variation of anisotropy in the inner core from PKP (BC)–PKP (DF) times. *J. Geophys. Res. Solid Earth* **102**, 2925–2938 (1997).
19. Irving, J. C. E. Imaging the inner core under Africa and Europe. *Phys. Earth Planet. Inter.* **254**, 12–24 (2016).
20. Przybilla, J., Wegler, U. & Korn, M. Estimation of crustal scattering parameters with elastic radiative transfer theory. *Geophys. J. Int.* **178**, 1105–1111 (2009).
21. Sato, H., Fehler, M. C. & Maeda, T. *Seismic Wave Propagation and Scattering in the Heterogeneous Earth*. **Vol. 496**, (Springer, 2012).
22. Kennett, B. L., Engdahl, E. R. & Buland, R. Constraints on seismic velocities in the Earth from traveltimes. *Geophys. J. Int.* **122**, 108–124 (1995).
23. Aubert, J., Amit, H., Hulot, G. & Olson, P. Thermochemical flows couple the Earth's inner core growth to mantle heterogeneity. *Nature* **454**, 758–761 (2008).
24. Mayeda, K. & Walter, W. R. Moment, energy, stress drop, and source spectra of western United States earthquakes from regional coda envelopes. *J. Geophys. Res. Solid Earth* **101**, 11195–11208 (1996).
25. Beghein, C. & Trampert, J. Robust normal mode constraints on inner-core anisotropy from model space search. *Science* **299**, 552–555 (2003).
26. Ishii, M. & Dziewoński, A. M. The innermost inner core of the earth: evidence for a change in anisotropic behavior at the radius of about 300 km. *Proc. Natl Acad. Sci. USA* **99**, 14026–14030 (2002).
27. Stephenson, J., Tkalčić, H. & Sambridge, M. Evidence for the innermost inner core: robust parameter search for radially varying anisotropy using the Neighbourhood Algorithm. *J. Geophys. Res. Solid Earth* **126**, e2020JB020545 (2021).
28. Yoshida, S., Sumita, I. & Kumazawa, M. Growth model of the inner core coupled with the outer core dynamics and the resulting elastic anisotropy. *J. Geophys. Res. Solid Earth* **101**, 28085–28103 (1996).
29. Deguen, R. & Cardin, P. Tectonic history of the Earth's inner core preserved in its seismic structure. *Nat. Geosci.* **2**, 419–422 (2009).
30. Huguet, L. Van, Orman, J. A., Hauck, S. A. II & Willard, M. A. Earth's inner core nucleation paradox. *Earth Planet. Sci. Lett.* **487**, 9–20 (2018).

31. Davies, C. J., Pozzo, M. & Alfè, D. Assessing the inner core nucleation paradox with atomic-scale simulations. *Earth Planet. Sci. Lett.* **507**, 1–9 (2019).
32. Sun, Y., Zhang, F., Mendelev, M. I., Wentzcovitch, R. M. & Ho, K. M. Two-step nucleation of the Earth's inner core. *Proc. Natl Acad. Sci. USA* **119**, e2113059119 (2022).
33. Lasbleis, M., Kervazo, M. & Choblet, G. The fate of liquids trapped during the Earth's inner core growth. *Geophys. Res. Lett.* **47**, e2019GL085654 (2020).
34. Labrosse, S. Thermal evolution of the core with a high thermal conductivity. *Phys. Earth Planet Inter.* **247**, 36–55 (2015).